AGU PUBLICATIONS

JGR

Journal of Geophysical Research: Solid Earth

RESEARCH ARTICLE
10.1002/2013JB010778

Key Points:
- Relaxation experiments mimic localization and reactivation
- Timing and energetics of rupture scale with an observable relaxation phase
- Method to compute time to failure based on observations of early-time response

Correspondence to:
S.-W. Hao,
haoshengwang@gmail.com

Citation:
Hao, S.-W., B.-J. Zhang, J.-F. Tian, and D. Elsworth (2014), Predicting time-to-failure in rock extrapolated from secondary creep, *J. Geophys. Res. Solid Earth*, *119*, 1942–1953, doi:10.1002/2013JB010778.

Received 16 OCT 2013
Accepted 12 FEB 2014
Accepted article online 15 FEB 2014
Published online 11 MAR 2014

Predicting time-to-failure in rock extrapolated from secondary creep

Sheng-Wang Hao[1,2,3], Bao-Ju Zhang[1], Ji-Feng Tian[1], and Derek Elsworth[2]

[1]School of Civil Engineering and Mechanics, Yanshan University, Qinhuangda, China, [2]Energy and Mineral Engineering, G[3] Center, and EMS Energy Institute, Pennsylvania State University, University Park, Pennsylvania, USA, [3]The State Key Laboratory of Nonlinear Mechanics, Institute of Mechanics, Chinese Academy of Science, Beijing, China

Abstract Stress relaxation experiments are reported that culminate in energetic failure in rocks analogous to the loading cycle and subsequent localization or reactivation on brittle faults embedded in an elastic medium. Universally, rapid primary deformation arrests and transitions into a long secondary deformation phase that ultimately accelerates to catastrophic rupture. Primary deformation (u) conforms to Andrade's law as $du/dt \sim (t_c - t_0)^{\theta}$ with a standard exponent of 2/3. In the long, and readily observable, secondary phase, the samples both deform and analogously shed load near linearly in time. This stress relaxation rate exhibits a robust power law dependency with time-to-rupture and exhibits the same 2/3 power law exponent observed in the primary phase. Similarly, the brittle strain energy released in the tertiary collapse scales with a normalized secondary stress relaxation rate. Together, these observations suggest a way to predict both the timing of rupture and its energetics from the observed stress (or strain) rate during the secondary relaxation stage.

1. Introduction

Delayed aftershocks and earthquake-earthquake interactions [*Parsons et al*., 2000] in the form of main shock-aftershock sequences have been well recognized but not well explained [*Parsons*, 2005]. Especially, the mechanisms and factors controlling the time delay are incompletely understood. Whether the Ya'an earthquake in Sichuan, southwest China's is an aftershock of the $M_w = 8$ Wenchuan earthquake (2008), or a separate event is part of this debate.

Static triggering [*King et al*., 1994; *Harris et al*., 1995; *Parsons*, 2002; *Lin and Stein*, 2004] and dynamic triggering [*Brodsky et al*., 2000; *Gomberg et al*., 2004; *Pankow et al*., 2004; *Prejean et al*., 2004; *Husen et al*., 2004; *Hill*, 2008; *Velasco et al*., 2008] are considered to be two primary forms of aftershock triggering. Static stress changes are calculated to increase and decrease failure stress in the region near the main shock [*King et al*., 1994], whereas dynamic stress changes are expected only to increase stress [*Parsons*, 2005]. Remotely triggered seismicity [*Hill et al*., 1993; *Prejean et al*., 2004; *Husen et al*., 2004] from the 2002 $M_w = 7.9$ Denali, Alaska earthquake, is commonly attributed to the passage of dynamic stress wave [*Freed*, 2005]. Triggering at such distances challenges the notion of causality by dynamic stress as the elastic stress change is far smaller than those caused even by lunar tides [*Freed*, 2005]. The observation of *Durand et al*. [2010] on the evolution of seismicity along the North Anatolian Fault and in the clusters neighboring the fault before and after the two large earthquakes of 1999, indicated that clusters can indeed be activated at large distances. Remarkably, their triggering is not immediately after the earthquake but is delayed with peak seismic activity occurring weeks or months after the triggering earthquake. Also, modeling studies of dynamic stress changes conclude that earthquakes are triggered as seismic waves pass through the crust, or very shortly thereafter [*Gomberg et al*., 1998; *Belardinelli et al*., 2003], implying that dynamic waves are not responsible for delayed aftershock sequences [*Parsons*, 2005]. Thus, current hypotheses of dynamic stress triggering do not explain delayed earthquake triggering and Omori's law [*Parsons*, 2005].

It is commonly accepted that viscoelastic behavior may be responsible for temporally delayed triggering. Field observations and theoretical results indicate that stress relaxation is related to earthquake rupture phenomena [*Richards*, 1976; *Reid*, 1910; *Turcotte and Shcherbakov*, 2006], which typically result from the release of strain energy stored in the surrounding medium [*Benioff*, 1951; *Salamon*, 1970; *Jaeger and Cook*, 1979]. Stress relaxation has been applied to the understanding of timing and distribution of seismic aftershock sequences [*Benioff*, 1951; *Turcotte and Shcherbakov*, 2006] with extensive observations indicating

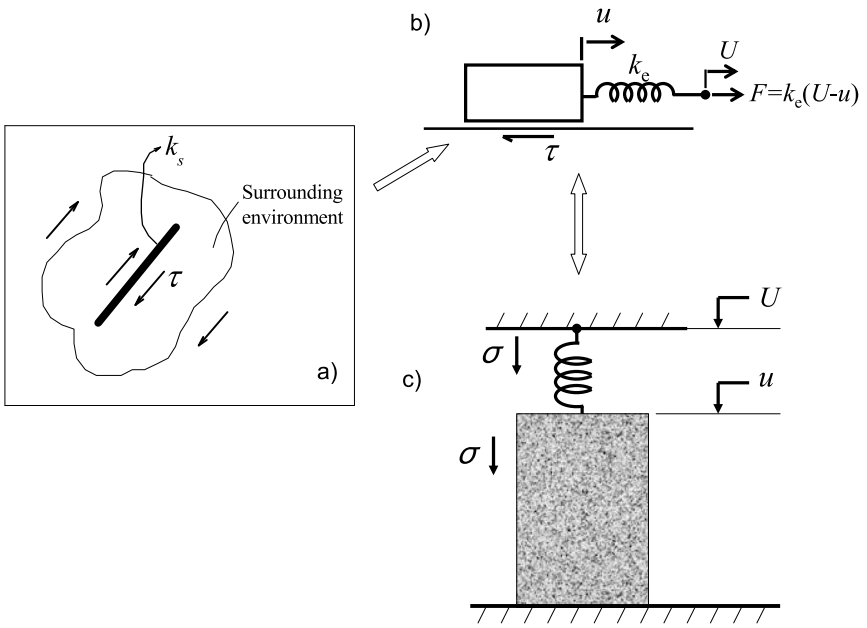

Figure 1. A schematic representation of energy release inducing instability. (a) Shear fault modeled as planar surface of (slip) displacement in elastic surrounding, (b) single-degree-of-freedom fault model, and (c) a system consisting of a linear spring and a damageable part in series used to describe energy release inducing instability.

that the relaxation process commonly involves rupture across a planar fault surface [*Reid*, 1910; *Richards*, 1976], and that earthquakes are the immediate result of some stress relaxation process [*Reid*, 1910; *Richards*, 1976]. The reappraisal of existing data suggests that stresses may begin to relax even before the coseismic rupture of the fault [*Gao and Crampin*, 2004].

During an earthquake, the surrounding regions in the vicinity of the fault-rupture experience a rapid increase in strain with dynamic strain transients radiating to the far field [*Velasco et al*., 2008]. Both of these near- and far-field effects are analogous to an instantaneously applied deformation [*Benioff*, 1951; *Turcotte and Shcherbakov*, 2006] in stress relaxation tests. *Parsons* [2005] presented a hypothesis for delayed dynamic earthquake triggering and showed numerically that if seismic waves can alter some frictional contacts in neighboring fault zones, then dynamic triggering might cause delayed triggering and an Omori law response. Thus, triggering is not expected to be instantaneous with the perturbation but would be delayed until the evolution to failure is complete [*Parsons*, 2005]. Tectonic shear faults are typically represented as planar surfaces of (slip) displacement within elastic surroundings (shown as Figure 1a) [*Brace and Byerlee*, 1966; *Rice*, 1983]. Where failure is reactivated on a preexisting fault, this geometry may be represented as a single-degree-of-freedom system (Figure 1b) or an analogous geometry where localization has yet to occur (Figure 1c). The release of stored elastic energy in the surroundings (represented by the spring in Figure 1b) will drive the sliding instability under some condition of slip weakening.

Stress transfer between faults through viscous relaxation may be a general cause of earthquake clustering [*Freed*, 2005]. *Casarotti and Piersanti* [2003] showed that the viscoelastic relaxation of the asthenosphere following major earthquakes that occurred in the past 60 years along the South American arc decreased Coulomb stress, thus inducing two seismic gaps near southern Peru and north Chile [*Freed*, 2005]. Viscoelastic relaxation following the 1944 $M_w = 8.0$ Tonankai and the 1946 $M_w = 8.2$ Nankaido, Japan, earthquakes has been shown to have slowly reduced clamping stresses on the Nojima Fault, inducing the 1995 $M_w = 6.9$ Kobe earthquake [*Pollitz and Sacks*, 1997].

Thus, stress relaxation may highlight the mechanism of aftershocks and delayed earthquake interactions. Understanding the process of stress relaxation rupture has the potential to provide insights into the physics of aftershocks and delayed earthquakes, and most importantly, clues of time-to-failure in stress relaxation rupture may greatly improve estimates of time delay.

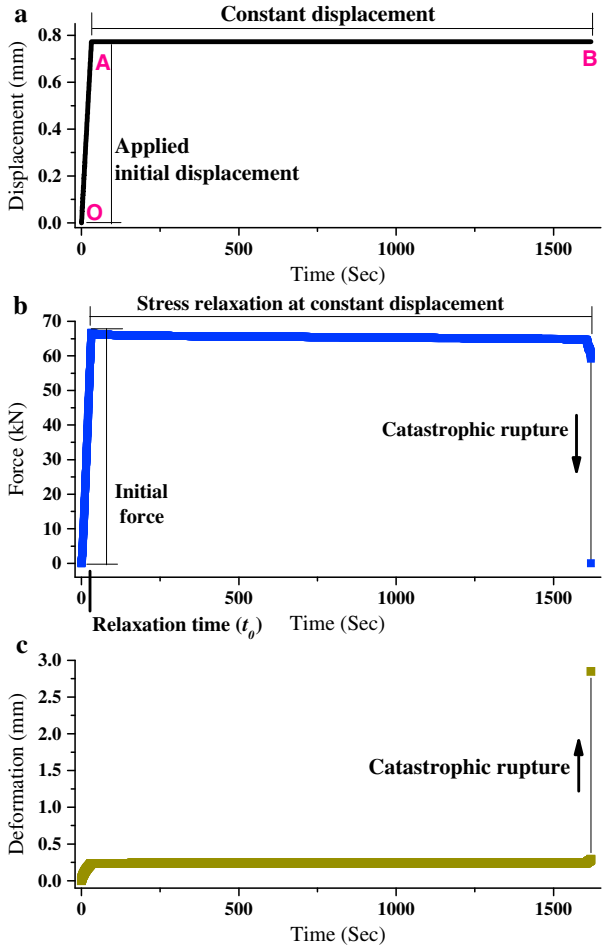

Figure 2. An example of catastrophic rupture observed in stress relaxation in granite. (a) Crosshead displacement versus time. The displacement remains constant after applying the initial displacement. (b) Force-time curve. The relaxation time t_0 denotes the time of peak force, which decreases thereafter with time. (c) Deformation of a tested sample over time. The arrow denotes the direction of the jump in force and deformation associated with a sudden catastrophic rupture.

Prior studies of time-to-failure in rocks have primarily focused on creep processes, which relate to the response under applied and invariant stresses [*Scholz*, 1968; *Du and McMeeking*, 1995; *Singh*, 1975; *Lockner*, 1993a, 1993b; *Heap et al*., 2011; *Benioff*, 1951; *Lienkaemper et al*., 1997] and is used as an analog for some processes of fault weakening that may lead to seismic rupture. Conversely, stress relaxation [*Benioff*, 1951; *Dupeux et al*., 1987; *Palt and Saha*, 1982] describes how materials under constant far-field deformation relieve stress, and relates more directly to the mode of loading typically conceived for the constant rate of far-field loading conceived for tectonic faults. This better defines the ultimate mode of energy release—strain softening versus strain hardening—that modulates the energetics of dynamic rupture. In reality, creep and relaxation behaviors are mere end-members of the pure stress and displacement loading conditions expected in nature—thus, observed behaviors in these modes are both analogous and complementary. Of particular interest in this is in understanding time-to-failure, as a function of precursive observations of deformation or of seismicity and in defining the energetics of the resulting failure, once failure occurs.

Creep failure in rock is typically classified within three temporal stages: primary creep, secondary creep, and finally accelerating tertiary creep as a precursor to failure [*Scholz*, 1968; *Lockner*, 1993a; *Boukharov et al*., 1995]. Early stage primary and tertiary creep are of particular interest as the form and rates of deformation may contain precursory information on the timing and energetics of ultimate failure. Primary creep typically conforms to Andrade's law [*da Andrade*, 1910] as an analog to Omori's law [*Omori*, 1894] observed in seismicity. Secondary creep provides the transition to tertiary creep that represents rapid, unstable growth, and thus, it should provide insight into the failure process. Power law acceleration during tertiary creep has been observed as a fundamental, but enigmatic, mode of material rupture [*Voight*, 1988b, 1989; *Guarino et al*., 2002; *Nechad et al*., 2005]. And similar power law accelerations are observed for landslides [*Saito and Uezawa*, 1961; *Saito*, 1969; *Petley et al*., 2002; *Amitrano et al*., 2005] and volcanoes [*Voight*, 1988a] as they approach criticality. Relating precursory deformations to failure in a predictive manner is an important goal.

During secondary creep, the strain rate is nearly constant and strongly dependent on the applied stress [*Amitrano and Helmstetter*, 2006]. An exponential relation of the average time-to-failure and the applied stress has been suggested [*Wiederhorn and Bolz*, 1970; *Das and Scholz*, 1981]. In this the time-to-failure of heterogeneous brittle materials decreases with an increase in the mean stress [*Scholz*, 1968, 1972; *Cruden*, 1974; *Kranz*, 1980; *Kranz et al*., 1982; *Boukharov et al*., 1995; *Baud and Meredith*, 1997; *Lockner*, 1998; *Di Giovambattista and Tyupkin*, 2001; *Masuda*, 2001; *Ciliberto et al*., 2001; *Purnell et al*., 2001; *Guarino et al*., 2002]. Crucially, the dependence of both secondary creep rate and time-to-failure on applied stress suggests that

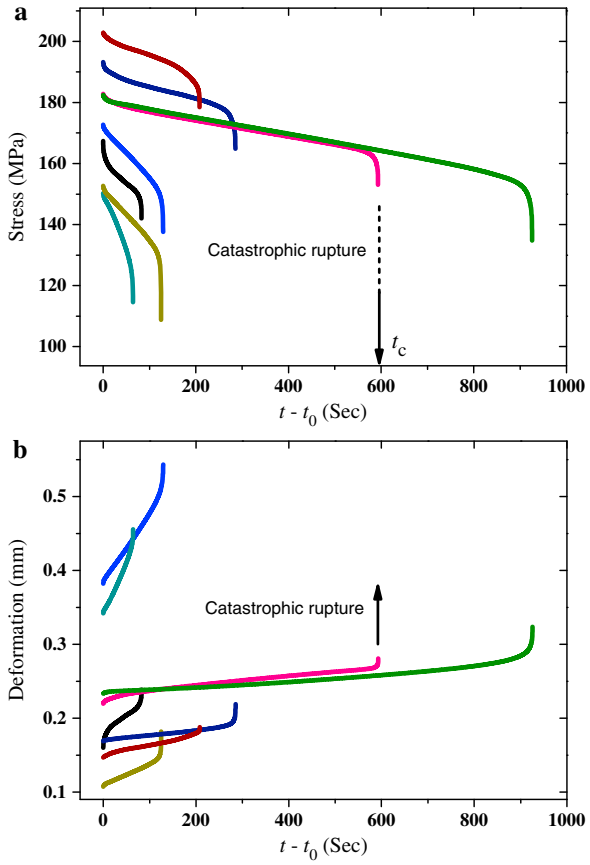

Figure 3. Experimental results of stress relaxation-inducing catastrophic rupture in the other eight rock samples. The arrow indicates the time to catastrophic rupture t_c for one example. (a) Temporal evolution of force. (b) Temporal evolution of deformation.

there should be a relationship between the secondary creep stage and the time-to-failure. Importantly, this relation may suggest a way to predict the timing and energetics of rupture from the observed stress (or strain or displacement) rate during secondary creep and before the accelerating accumulation of damage that ultimately leads to rupture.

A recent analytical study [*Hao et al.*, 2012] of a heterogeneous system, consisting of an elastic component and a damageable component in series, describes rupturing under gradual stress relaxation. This shows [*Hao et al.*, 2012] that global creep rupture could occur during relaxation if the elastic energy stored in the elastic component exceeded the fracture energy of the damageable component. This work rationalized this gradual and ultimate failure but did not prescribe a rationale for the ultimate catastrophic rupture. Observations are required to understand the different evolution stages of stress (or strain) during the process and to explore a way to predict time-to-failure. The crucial need is a relation between the evolution of observable proxies (deformation or strain) during the secondary relaxation stage and both time-to-failure (or time delay of aftershocks) and failure modes. This is important because the evolution properties in the secondary stage represent the ability of the system to dissipate energy before the unstable acceleration to failure in the tertiary stage and thus may dominate the duration of the time delay of aftershocks and even determine their occurrence.

To understand the time-dependent process of elastic energy release-inducing dynamic rupture in rock and to simulate the time delay process of near-field aftershocks and earthquake interactions induced by the instantaneous increase in strain resulting from the main shock, a system consisting of a linear spring and a damageable specimen in series (Figure 1c) [*Salamon*, 1970; *Hudson et al.*, 1972; *Jaeger and Cook*, 1979; *Hao et al.*, 2012] is used in this work. This specimen is subjected to a rapid compression (to simulate a large displacement step after a nearby earthquake or a seismic wave pulse) that is then held constant, allowing stresses to relax with the accumulation of damage. The experiments enable observation of how energy release drives creep failure during stress relaxation and to understand the evolution of stress (strain) rates. Although defining and commenting upon the scaling laws within the primary and tertiary stages, we mainly focus on the relationship between secondary stage deformation rates and their relation to both time-to-failure and their relation with the energetics of brittle strain energy release.

2. Experimental Methodology and Material

Relaxation experiments are conducted on prismatic blocks cut to 16 mm × 20 mm × 40 mm. The rock samples are from Beijing, China, from a depth of ~10 m. These samples are surface ground for parallelism and perpendicularity between the faces and in particular to confirm that the two ends are exactly perpendicular to the longitudinal axis of the sample. The samples are intact but with many intrinsic and natural microfractures randomly distributed within the sample. Uniaxial (unconfined) compression tests are performed at room

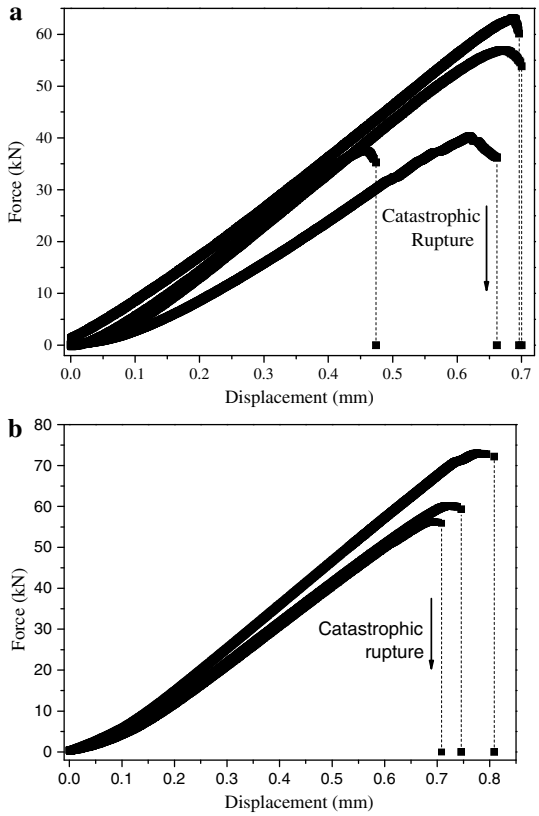

Figure 4. Dynamic rupture in rocks under monotonic loading at constant displacement rate (0.05 mm/min). (a) Marble and (b) granite. The samples fail suddenly in the postfailure stage at peak force. Marble exhibits a larger scatter in peak force and failure displacement than granite. The displacements in the stress relaxation tests are selected as the average displacement at peak force in these monotonic tests.

temperature using a screw-driven crosshead, universal electromechanical testing machine equipped with a force sensor with an offset load of 1 kN. The deformation u of a specimen is measured with a resolution of 1 μm located on the sides of the tested specimens. In the experiments, two types of rock samples (granite and marble) are compressed uniaxially along the 40 mm axis.

The machine uses real-time closed-loop displacement control with all specimens rapidly loaded to the initial deformation state (part *OA* in Figure 2a) for the subsequent relaxation test. This involves limiting the ultimate crosshead displacement of the apparatus to ~0.74 mm for granite and ~0.68 mm for marble, with a crosshead speed of 1.5 mm/min. The crosshead is then held to this constant position (part *AB* in Figure 2a) in both specimen types and displacement of the sample is measured as it relaxes.

The experimental arrangement involves a crosshead that remains stationary (zero net displacement) but that encases a sample and elastic member in series that may strain sympathetically—as the sample sustains damage, it shortens, the stiff elastic member lengthens, and the stress relaxes. Thus, the compressive displacement (U) at the crosshead of the testing machine combines [*Salamon*, 1970; *Hudson et al*., 1972; *Jaeger and Cook*, 1979; *Hao et al*., 2012] the deformation of the loading apparatus (u_m) and of the deformed rock sample (u). Thus, the load apparatus accumulates substantial elastic energy at the stage of the applied initial displacement. The deformation of the specimen cannot then remain constant [*Aifantis and Gerberich*, 1975; *Hao et al*., 2010] during stress relaxation because there is elastic recovery of the loading apparatus. Therefore, an infinitely rigid test apparatus would be needed to obtain the true stress relaxation characteristics of a material [*Aifantis and Gerberich*, 1975; *Sinha and Sinha*, 2005]. Instead, we can take advantage of the elasticity of the testing machine to represent the surrounding and compliant elastic environment that occurs in nature.

The stiffness of the loading apparatus is ~130 kN/mm, and catastrophic rupture was observed in all nine rock specimens that were loaded. Figure 2 shows the results when using a granite specimen. As shown, the displacement is held constant after the crosshead reaches the initial position (Figure 2a), with stress relaxation then accompanying the increase of deformation in the specimen (Figures 2b and 2c). Thus, rock samples undergo a combination of creep and stress relaxation.

3. Results

3.1. Stress, Strain Level and Dependence of Time-to-Failure on Stiffness of Testing Machine, and Initially Applied Displacement

A total of 67 samples (32 marble and 35 granite) are loaded in stress relaxation tests with different initial displacements. Some samples fail immediately during the application of the initial displacement—these experiments are discarded as they produce no data. Some samples do not fail during the available time

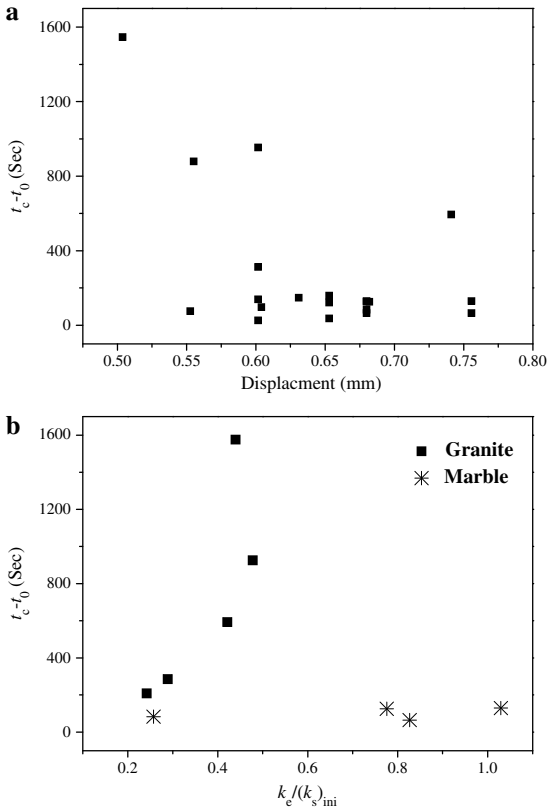

Figure 5. Dependence of time-to-failure on stiffness of the testing machine and the applied displacement. (a) Dependence of time-to-failure on the applied displacement for marble. (b) Stiffness of testing machine versus time-to-failure for granite and marble samples subject to the same displacement, where k_e is the stiffness of testing machine and $(k_s)_{ini}$ represents the initial stiffness of the rock samples.

window of 5 days—these experiments are discarded. Following this calibration (23 experiments) for the distribution of sample strengths, we conduct nine tests with prescribed initial displacements (0.74 mm for granite and 0.68 mm for marble) with results shown in Figures 2 and 3. These experiments show a large variability in the time to catastrophic rupture t_c between various samples (Figure 3) but for the same imposed displacement. In Figure 2, t_0 is defined as the starting time of the stress relaxation and thus is both the point of maximum stress σ_{max}, and the onset of initial displacement, during which the load apparatus begins to shed its substantial elastic energy. It is the release of this energy during the process of stress relaxation that promulgates further damage and ends in catastrophic rupture.

The initial calibration uses 23 samples (13 marbles and 10 granites) compressed under monotonic loading by setting the crosshead displacement at 0.05 mm/min with loading to failure (i.e., no hold step). Figure 4 shows the representative displacement-force curves for marble and granite as examples. It can be seen that the samples fail suddenly at some point in the postfailure stage after peak force. Marble exhibits a larger scatter of both peak force and displacement at failure than granites, although all rock samples present individual behaviors of either evolution of the force-displacement curve or the failure displacement and peak forces. The selected applied displacements in the stress relaxation tests are almost equal to the failure displacements in the monotonic tests and the maximum force at t_0 is almost equal to the peak force in the monotonic tests.

As shown in Figures 2 and 3, the maximum stresses at relaxation time t_0 (as defined in Figure 2) range from 182.5 MPa to 208.4 MPa for granite and 150.2 MPa to 172.7 MPa for marble. The failure stresses are 134.8 MPa to 178.5 MPa for granite and 108.8 MPa to 142.02 MPa for marble. The applied stress level is higher for granite than for marble but the strain level at maximum stress is smaller for granite (3670 με to 5800 με) than for (2680 με to 9500 με). This difference results from the lower stiffness for the marble relative to granite (see Figure 5a).

To present a clear explanation of the dependence of time-to-failure on the applied initial displacement, Figure 5a shows the results for marble under different displacements. The time-to-failure decreases with increased displacement but with some scatter (Figure 3) modulated by heterogeneity. The scatter is very large when the displacement is 0.602 mm as shown in Figure 5a.

It is worth mentioning that catastrophic rupture is controlled by three factors: the stiffness ratio between the load apparatus and the rock sample, the initial applied displacement and the damage evolution properties of the rock. The stiffness ratio and the initial applied displacement determine the initial stored energy in the load apparatus. The damage evolution properties determine the stress (or deformation, displacement)-time curves of the rock. Therefore, the stiffness of the testing machine plays an important role in promoting failure. We calculate the specific ratio (as shown in Figure 5b) between the stiffness k_e of the machine and the initial stiffness $(k_s)_{ini}$ of every sample according to the almost linear force-deformation relations in the stage of applying the initial displacement. The stiffness of the testing machine varies from 117.0 kN/mm to 156.7 kN/mm during the stress relaxation tests with the initial stiffnesses of the samples exhibiting

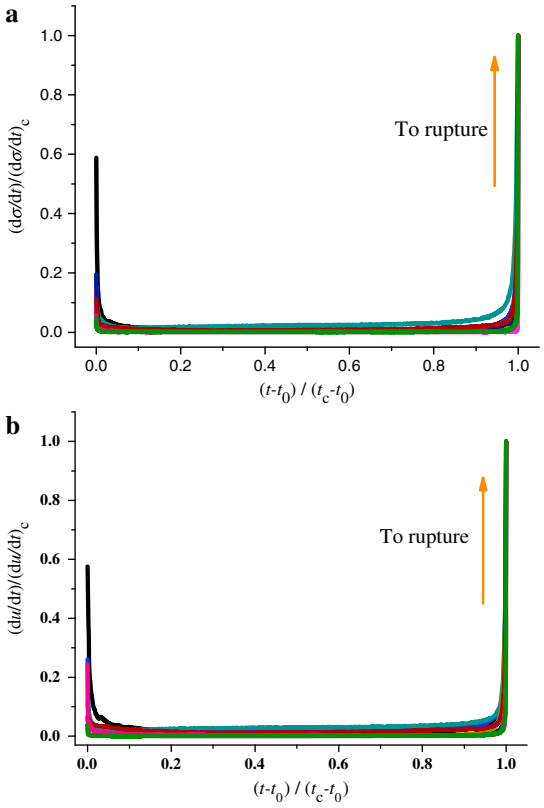

Figure 6. Stress relaxation and deformation rate evolutions for all nine samples. (a) Evolution curves of force rate dσ/dt normalized by their corresponding values $(d\sigma/dt)_c$ versus time $(t - t_0)/(t_c - t_0)$ for all nine rock samples. (b) Evolution curves of deformation rate du/dt normalized by their corresponding values $(du/dt)_c$ versus time $(t - t_0)/(t_c - t_0)$ for all nine rock samples.

a larger scatter. Since the time-to-failure is a complex combination of machine stiffness and initial sample stiffness effects, it is not possible to decouple the combined effects of testing machine and rock sample for these five (granite) or four (marble) samples to present a statistically explicit relationship between stiffness of testing machine and failure time.

3.2. Stages of Stress Relaxation Creep and the Scaling Laws in Primary and Tertiary Stages

A typical stress relaxation process is described as the rapid initial relaxation of stress, followed by a slow relaxation stage in which the stress decreases at a constant rate. This constant rate of stress relief terminates abruptly by an acceleration of stress loss and deformation that often culminates in catastrophic failure (Figure 2b and 2c). The results imply that, in heterogeneous brittle materials, stress relaxation may induce catastrophic rupture if the elastic energy stored in the surrounding environments can compensate for the fracture energy of a specimen.

It is observed that catastrophic rupture associated with stress relaxation follows a temporal sequence comprising three stages (see Figures 2b, 2c, 3, and 6) of primary, then secondary, then terminal relaxation, to failure. All rock specimens tested showed this characteristic response including a transient decrease of the stress relaxation rate and the deformation rates, similar to the so-called primary creep regime or Andrade creep regime [*da Andrade*, 1910]. This is followed by a steady state relaxation stage, in which the deformation-time and related stress-time curves exhibit an approximately constant slope. The sequence ends with the accelerating evolution of stress and deformation that leads rapidly to catastrophic rupture.

The decrease of the initial deformation rate du/dt (and the corresponding stress rate) in the first stage can be described by Andrade's law [*da Andrade*, 1910] $du/dt \sim (t - t_0)^{-\theta}$ ($|d\sigma/dt| \sim (t - t_0)^{-\theta}$), with an exponent $\theta \approx 2/3$ (as shown in Figures 7a and 7b). This is in agreement with Andrade's original observations [*da Andrade*, 1910] and those of *Miguel et al.* [2003].

In the third stage of tertiary and ultimately terminal relaxation, the accelerating drop in stress, together with the rapid increase in deformation, exhibits a power law singularity $du/dt \sim (t_c - t)^{-\beta}$ or $|d\sigma/dt| \sim (t_c - t)^{-\beta}$ prior to rupture(Figures 7c and 7d), where t_c represents the catastrophic time for the sample.

3.3. The Dependence of Time-to-Failure and Failure Modes on Secondary Stage Deformations

Energy release together with damage evolution of the rock sample determines the rate of stress relaxation and thus the lifetime of the sample t_c and the stress relaxation slope of the secondary stage. The secondary stage of deformation dominates the entire lifetime of the specimen. In the experiments, a steep stress relaxation slope in the secondary stage implies a short lifetime with the lifetime represented by a power law relationship. The stress relaxation slope λ_s of the secondary stage is shown in Figure 8 with an exponent of approximately $-2/3$: $(t_c - t_0) \sim (-\lambda_s)^{-2/3}$.

Figure 9a shows the dependence of the ratio $-\lambda_s/(\sigma_{max}/(t_c - t_0))$ on total stored energy in the system at t_0, where σ_{max} is the maximum stress at t_0. The value of $-\lambda_s/(\sigma_{max}/(t_c - t_0))$ ranges from 0 to 1 and large

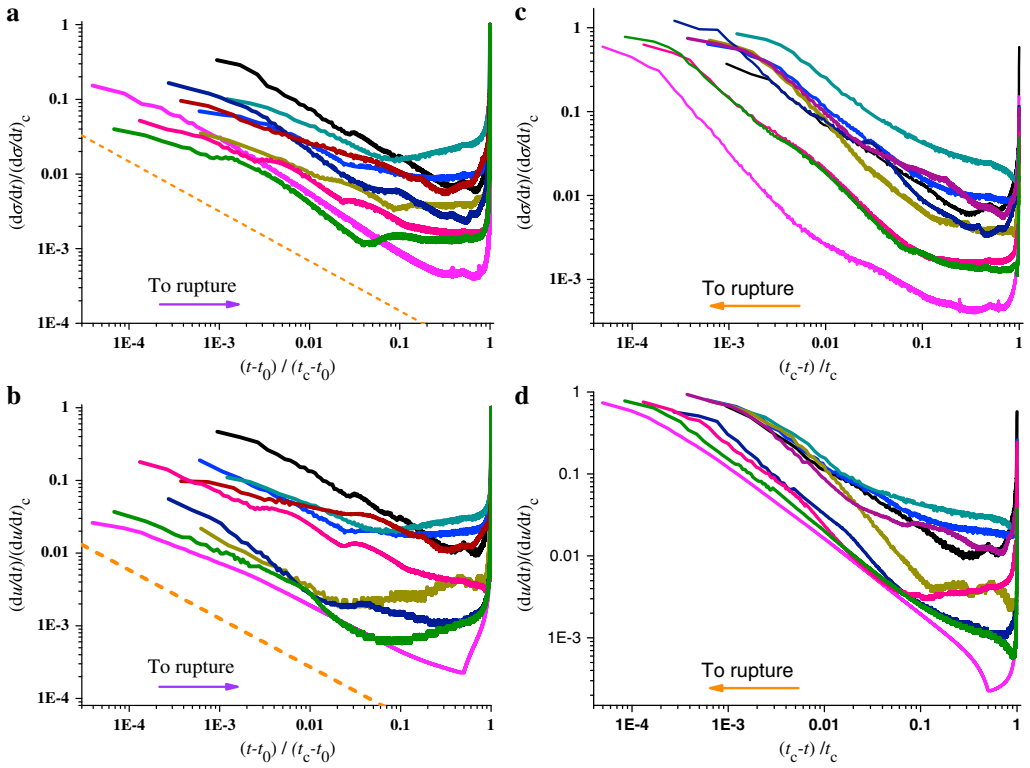

Figure 7. Scaling law in primary and tertiary stages. (a and b) Logarithmic timescale $(t - t_0)/(t_c - t_0)$ to test for Andrade's law in the primary stage, dashed line with slope −2/3 is drawn for comparison. And (c and d) logarithmic timescale $(t_c - t)/t_c$ indicates the power law behavior of stress and deformation prior to catastrophic rupture. (Figure 7a) Log-log plots of stress rate $d\sigma/dt$ normalized by corresponding values $(d\sigma/dt)_c$ at catastrophic rupture versus time $(t - t_0)/(t_c - t_0)$. (Figure 7b) Log-log curve of deformation rate du/dt normalized by corresponding values $(du/dt)_c$ at catastrophic rupture versus time $(t - t_0)/(t_c - t_0)$. (Figure 7c) Log-log plots of stress rate $d\sigma/dt$ normalized by corresponding values $(d\sigma/dt)_c$ at catastrophic rupture versus time $(t_c - t)/t_c$. (Figure 7d) Log-log curve of deformation rate du/dt normalized by corresponding values $(du/dt)_c$ at catastrophic rupture versus time $(t_c - t)/t_c$.

$-\lambda_s/(\sigma_{max}/(t_c - t_0))$ represents that the slope $-\lambda_s$ of the secondary relaxation is closer to $\sigma_{max}/(t_c - t_0)$. During the process of relaxation, the energy dissipation is directly proportional to force because it is equal to $(FU)/2$ and U is constant. So a lower value of $-\lambda_s/(\sigma_{max}/(t_c - t_0))$ represents the case where the system dissipates relatively less energy before rupture. This may result in a more quiescence precursor, but consequently, the eventual rupture may be more brittle and sudden. Thus, the closer the relaxation slope in the secondary stage to $\sigma_{max}/(t_c - t_0)$ represents a weaker rock and a less brittle failure. In other words, high stored energy in a system under the same imposed displacement U will result in a more brittle rupture because the ratios $-\lambda_s/(\sigma_{max}/(t_c - t_0))$ decrease with an increment of the stored energy.

4. Discussion and Conclusions

We have experimentally verified that violent catastrophic rupture can be induced during the process of stress relaxation. This occurs during a tertiary stage, characterized by accelerated stress relaxation which leads to the complete rupture of the specimen. Furthermore, the accelerated processes of deformation and stress evolution can be described as a power law response. The time-to-failure shows dependence on the initial applied displacements and the stiffness ratio of the testing machine and samples. However, these experiments cannot provide an explicit relation between the coupled effects of the stiffness of the testing machine and the stress evolution of the rock samples. This is because the damage (or stress) evolution of the rock is sample specific. Thus, these experiments show a large variability in the time to catastrophic rupture between various samples but for the same imposed displacement. This highlights the role of sample

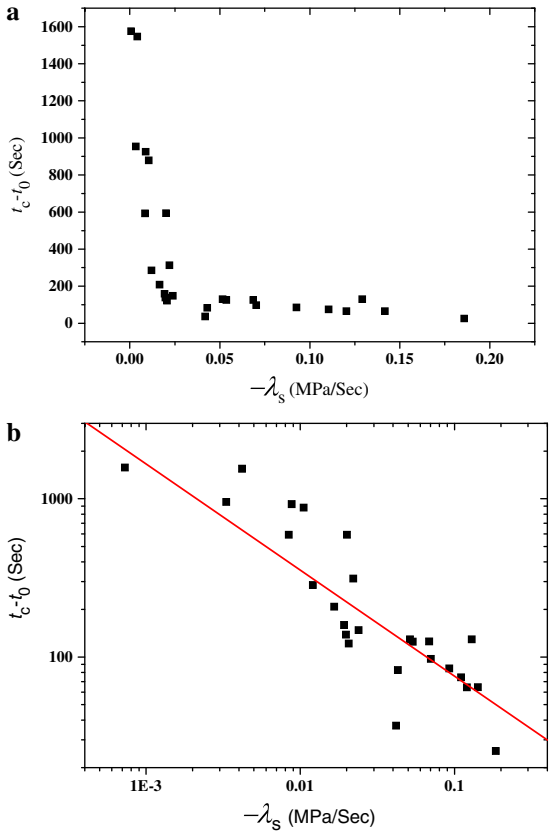

Figure 8. Relationship between the stress relaxation slopes λ_s of secondary stage and lifetimes $(t_c - t_0)$. (a) Lifetime versus slope curve, and (b) on a log-log scale to show a power law relation: $(t_c - t_0) \sim \lambda_s^{-2/3}$. The solid straight line is the fitted result.

heterogeneity in predicting the timing of rupture or the time delay of aftershocks even in a controlled laboratory experiment.

However, we find that the lifetimes of rock samples may be represented by a power law dependent on the stress relaxation slope of the secondary stage. This may also provide a means to predict the time delay to failure similar to delayed aftershocks and earthquake interaction. A steep slope of the secondary relaxation means a high value of $\sigma_{max}/(t_c - t_0)$ (Figure 9b) and indicates a short lifetime (Figure 8). Under the same imposed displacement U, this high-energy state represents a low ratio of $-\lambda_s/(\sigma_{max}/(t_c - t_0))$ and implies a more brittle rupture. These observations have important implications regarding the long-term behavior of heterogeneous material. This is because most published studies in these areas divide stress relaxation into only two stages: the primary stage is followed by a steady state in which stress asymptotically tends to a constant value, with rate of stress reduction tending to approach zero with time.

For a plastic material undergoing stress relaxation, the initial imposed elastic strain is replaced over time by inelastic strain [*Aifantis and Gerberich*, 1975; *Lloyd et al*., 1970; *Sinha and Sinha*, 2005], and thus, the stress relaxes with time. However, for heterogeneous brittle materials such as rock or concrete, the drop in force is induced by damage that then relaxes the stress. The time delay until the occurrence of damage is associated with crack initiation and propagation [*Turcotte and Shcherbakov*, 2006], and the coalescence and growth of microcracks and microdefects that ultimately leads to the development into macroscale fractures.

Energy release of the elastic surround drives the damage propagation and thus induces the weakness of the rock sample, which eventually leads to catastrophic rupture. Even in very stiff machines, localization may also lead to catastrophic rupture during stress relaxation. This may result when localization leads to bifurcation of the material into two media—a soft localized zone and a stiffer elastic surround that retain much of the strain

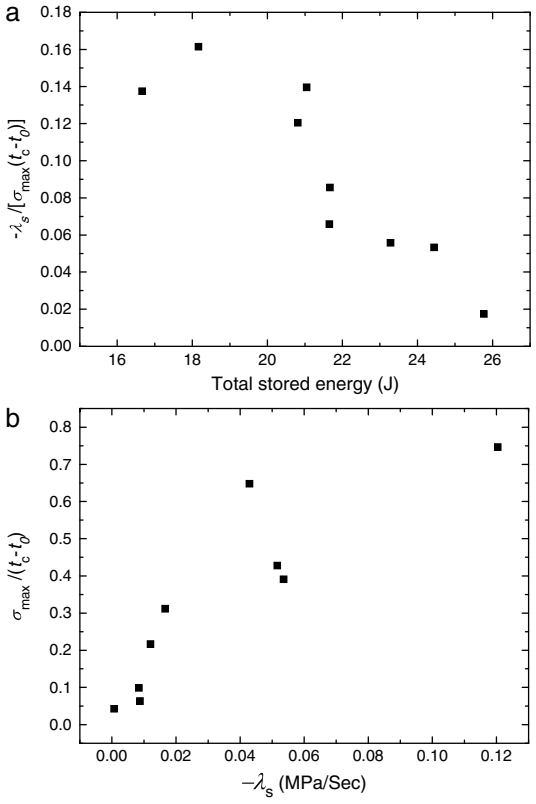

Figure 9. Relationship of the stress relaxation slopes λ_s of stored energy and lifetimes $(t_c - t_0)$. (a) Dependence of ratio $\lambda_s/(\sigma_{max}/(t_c - t_0))$ on total stored energy. Under a same imposed displacement U, high-energy state means a low ratio of $\lambda_s/(\sigma_{max}/(t_c - t_0))$ and implies a more brittle rupture. (b) Dependence of $\sigma_{max}/(t_c - t_0)$ on λ_s. A steep slope of the secondary relaxation means a high value of $\sigma_{max}/(t_c - t_0)$.

energy [*Labuz and Biolzi*, 1991; *Rathbun and Marone*, 2010; *Hao et al*., 2010]. As soon as the elastic energy stored in zones outside the localized zone becomes greater than the fracture energy of the localized zone, then catastrophic rupture will occur during stress relaxation.

In this application, the laboratory testing system is equivalent to the diffuse zones following localization in the material which will release stored strain energy during the long-term stress relaxation process. Thus, the findings have important implications for fields such as seismology and rock-mass stability. In this it is suggested that seismic aftershocks may be attributed to such processes of stress relaxation [*Benioff*, 1951; *Turcotte and Shcherbakov*, 2006] and that recent earthquakes may indeed merely be aftershocks from large earthquakes that occurred centuries ago [*Stein and Liu*, 2009]. Many major faults, including the San Andreas Fault, are weak compared with the surrounding rock [*Carpenter et al*., 2011]. The surrounding rock stores substantial strain energy that is released during the stress relaxation after the main shock (or dynamic stress) induces rupture, i.e., an aftershock in the near field (or remote field). The present results in this paper may therefore help explain the triggering mechanism of some natural ruptures and explain the decrease in precursory events [*Gao and Crampin*, 2004] before the event.

Acknowledgments
This work is supported by National Basic Research Program of China (grant 2013CB834100). We acknowledge useful comments of Editor, Tom Parsons, and two anonymous reviewers.

References

Aifantis, E. C., and W. W. Gerberich (1975), A theoretical review of stress relaxation testing, *Mater. Sci. Eng.*, *21*, 107–1137.
Amitrano, D., and A. Helmstetter (2006), Brittle creep, damage and time to failure in rocks, *J. Geophys. Res.*, *111*, B11201, doi:10.1029/2005JB004252.
Amitrano, D., J. Grasso, and G. Senfaute (2005), Seismic precursory patterns before a cliff collapse and critical point phenomena, *Geophys. Res. Lett.*, *32*, L08314, doi:10.1029/2004GL022,270.
Baud, P., and P. Meredith (1997), Damage accumulation during triaxial creep of darley dale sandstone from pore volumetry and acoustic emission, *Int. J. Rock Mech. Min. Sci. Geomech. Abstr.*, *34*(3-4), 1–8.
Belardinelli, M. E., A. Bizzarri, and M. Cocco (2003), Earthquake triggering by static and dynamic stress changes, *J. Geophys. Res.*, *108*(B3), 2135, doi:10.1029/2002JB001779.
Benioff, H. (1951), Earthquake and rock creep, *Bull. Seismol. Geol. Soc. Am.*, *41*(1), 31–62.
Boukharov, G., M. Chanda, and N. Boukharov (1995), The three processes of brittle crystalline rock creep, *Int. J. Rock Mech. Min. Sci. Geomech. Abstr.*, *32*(4), 325–335.
Brace, W. F., and J. D. Byerlee (1966), Stick-slip as a mechanism for earthquakes, *Science*, *153*, 990–992.
Brodsky, E. E., V. Karakostas, and H. Kanamori (2000), A new observation of dynamically triggered regional seismicity: Earthquakes in Greece following the August, 1999 Izmit, Turkey earthquake, *Geophys. Res. Lett.*, *27*, 2741–2744.
Carpenter, B. M., C. Marone, and D. M. Saffer (2011), Weakness of the San Andreas Fault revealed by samples from the active fault zone, *Nat. Geosci.*, *4*, 251–254, doi:10.1038/ngeo1089.
Casarotti, E., and A. Piersanti (2003), Postseismic stress diffusion in Chile and South Peru, *Earth Planet. Sci. Lett.*, *206*, 325–333.
Ciliberto, S., A. Guarino, and R. Scoretti (2001), The effect of disorder on the fracture nucleation process, *Phys. D*, *158*(1-4), 83–104.
Cruden, D. (1974), The static fatigue of brittle rock under uniaxial compression, *Int. J. Rock Mech. Min. Sci. Geomech. Abstr.*, *11*, 67–73.
da Andrade, E. N. C. (1910), On the viscous flow in metals and allied phenomena, *Proc. R. Soc. London A*, *84*, 1.
Das, S., and C. H. Scholz (1981), Theory of time-dependent rupture in the Earth, *J. Geophys. Res.*, *86*, 6039–6051.
Di Giovambattista, R., and Y. Tyupkin (2001), An analysis of the process of acceleration of seismic energy in laboratory experiments on destruction of rocks and before earthquakes on Kamchatka and in Italy, *Tectonophysics*, *338*, 339–351.
Du, Z. Z., and R. M. McMeeking (1995), Creep models for metal matrix composites with long brittle fibers, *J. Mech. Phys. Solids*, *43*, 701–726.
Dupeux, M., J. Henriet, and M. Ignat (1987), Tensile stress relaxation behaviour of Ni-based superalloy single crystals between 973 and 1273 K, *Acta Metall.*, *35*(9), 2203–2212.

Durand, V., M. Bouchon, H. Karabulut, D. Marsan, J. Schmittbuhl, M. P. Bouin, M. Aktar, and G. Daniel (2010), Seismic interaction and delayed triggering along the North Anatolian Fault, *Geophys. Res. Lett.*, *37*, L18310, doi:10.1029/2010GL044688.

Freed, A. M. (2005), Earthquake triggering by static, dynamic, and postseismic stress transfer, *Annu. Rev. Earth Planet. Sci.*, *33*, 335–367, doi:10.1146/annurev.earth.33.092203.

Gao, Y., and S. Crampin (2004), Observations of stress relaxation before earthquakes, *Geophys. J. Int.*, *157*, 578–582.

Gomberg, J., N. M. Beeler, M. L. Blanpied, and P. Bodin (1998), Earthquake triggering by transient and static deformation, *J. Geophys. Res.*, *103*, 24,411–24,426.

Gomberg, J., P. Bodin, K. Larson, and H. Dragert (2004), Earthquake nucleation by transient deformations caused by the M = 7.9 Denali, Alaska, earthquake, *Nature*, *427*, 621–624.

Guarino, A., S. Ciliberto, A. Garcimartin, M. Zei, and R. Scoretti (2002), Failure time and critical behavior of fracture precursors in heterogeneous materials, *Eur. Phys. J. B*, *26*, 141–151, doi:10.1140/epjb/e20020075.

Hao, S. W., M. F. Xia, F. J. Ke, and Y. L. Bai (2010), Evolution of localized damage zone in heterogeneous media, *Int. J. Damage Mech.*, *19*, 787–804.

Hao, S. W., B. J. Zhang, and J. F. Tian (2012), Relaxation creep rupture of heterogeneous material under constant strain. *Phys. Rev. E*, *85*, 012501, doi:10.1103/PhysRevE.85.012501.

Harris, R. A., R. W. Simpson, and P. A. Reasenberg (1995), Influence of static stress changes on earthquake locations in southern California, *Nature*, *375*, 221–224.

Heap, M. J., P. Baud, P. G. Meredith, S. Vinciguerra, A. F. Bell, and I. G. Main (2011), Brittle creep in basalt and its application to time-dependent volcano deformation, *Earth Planet. Sci. Lett.*, *37*(1-2), 71–82.

Hill, D. P. (2008), Dynamic stresses, Coulomb failure, and remote triggering, *Bull. Seismol. Soc. Am.*, *98*, 66–92.

Hill, D. P., P. A. Reasenberg, A. J. Michael, W. J. Arabasz, and G. C. Beroza (1993), Seismicity remotely triggered by the magnitude 7.3 Landers, California earthquake, *Science*, *260*, 1617–1623.

Hudson, J. A., S. L. Crouch, and C. Fairhurst (1972), Soft, stiff and servo-controlled testing machines: A review with reference to rock failure, *Eng. Geol.*, *6*, 155–189.

Husen, S., S. Wiemer, and R. B. Smith (2004), Remotely triggered seismicity in the Yellowstone National Park region by the 2002 Mw = 7.9 Denali Fault Earthquake. Alaska, *Bull. Seismol. Soc. Am.*, *94*, S317–S331.

Jaeger, J. C., and N. G. W. Cook (1979), *Fundamentals of Rock Mechanics*, 3rd ed., pp. 308–309, Chapman and Hall, London.

King, G. C. P., R. S. Stein, and J. Lin (1994), Static stress changes and the triggering of earthquakes, *Bull. Seismol. Soc. Am.*, *84*, 935–953.

Kranz, R. L. (1980), The effects of confining pressure and stress difference on static fatigue of granite, *J. Geophys. Res.*, *85*, 1854–1866.

Kranz, R., W. Harris, and N. Carter (1982), Static fatigue of granite at 200°C, *Geophys. Res. Lett.*, *9*, 1–4.

Labuz, J. F., and L. Biolzi (1991), Class I vs class II stability : A demonstration of size effect, *Int. J. Rock Mech. Min. Sci. Geomech. Abstr.*, *28*, 199–205.

Lienkaemper, J. J., J. S. Galehouse, and R. W. Simpson (1997), Creep response of the Hayward Fault to stress changes caused by the Loma Prieta earthquake, *Science*, *276*, 2014–2016.

Lin, J., and R. S. Stein (2004), Stress triggering in thrust and subduction earthquakes and stress interaction between the southern San Andreas and nearby thrust and strike-slip faults, *J. Geophys. Res.*, *109*, B02303, doi:10.1029/2003JB002607.

Lloyd, D. J., P. J. Worthington, and J. D. Embury (1970), Dislocation dynamics in the copper-tin system, *Phil. Mag.*, *22*, 1147–1160.

Lockner, D. A. (1993a), The role of acoustic emission in the study of rock fracture, *Int. J. Rock Mech. Min. Sci. Geomech. Abstr.*, *30*(7), 883–899.

Lockner, D. A. (1993b), Room temperature creep in saturated granite, *J. Geophys. Res.*, *98*, 475–487.

Lockner, D. A. (1998), A generalized law for brittle deformation of westerly granite, *J. Geophys. Res.*, *103*, 5107–5123.

Masuda, K. (2001), Effects of water on rock strength in a brittle regime, *J. Struct. Geol.*, *23*, 1653–1657.

Miguel, M. C., J. S. Andrade Jr., and S. Zapperi (2003), Deblocking of interacting particle assemblies: From pinning to jamming, *Braz. J. Phys.*, *33*, 557–571.

Nechad, H., A. R. Helmstetter, E. Guerjouma, and D. Sornette (2005), Andrade creep and critical time-to-failure laws in heterogeneous materials, *Phys. Rev. Lett.*, *94*, 045,501, doi:10.1016/j.jmps.2004.12.001.

Omori, F. (1894), On the aftershocks of earthquakes, *J. Coll. Sci. Imp. Univ. Tokyo*, *7*, 111–120.

Palt, S., and S. Saha (1982), Stress relaxation and creep behaviour of normal and carbon fibre reinforced acrylic bone cement, *Biomaterials*, *3*(2), 93–96.

Pankow, K. L., W. J. Arabasz, J. C. Pechmann, and S. J. Nava (2004), Triggered seismicity in Utah from the November 3, 2002, Denali Fault earthquake, *Bull. Seismol. Soc. Am.*, *94*, S332–S347.

Parsons, T. (2002), Global Omori law decay of triggered earthquakes: Large aftershocks outside the classical aftershock zone. *J. Geophys. Res.*, *107*(B9), 2199 doi:10.1029/2001JB000646.

Parsons, T. (2005), A hypothesis for delayed dynamic earthquake triggering, *Geophys. Res. Lett.*, *32*, L04302, doi:10.1029/2004GL021811.

Parsons, T., S. Toda, R. S. Stein, A. Barka, and J. H. Dieterich (2000), Heightened odds of large earthquakes near Istanbul: An interaction-based probability calculation, *Science*, *288*, 661–665.

Petley, D., M. Bulmer, and W. Murphy (2002), Patterns of movement in rotational and translational landslides, *Geology*, *30*(8), 719–722, doi:10.1130/0091-7613.

Pollitz, F. F., and S. I. Sacks (1997), The 1995 Kobe, Japan, earthquake; a long-delayed aftershock of the offshore 1944 Tonankai and 1946 Nankaido earthquakes, *Bull. Seismol. Soc. Am.*, *87*, 1–10.

Prejean, S. G., D. P. Hill, E. E. Brodsky, S. E. Hough, M. J. S. Johnston, S. D. Malone, D. H. Oppenheimer, A. M. Pitt, and K. B. Richards-Dinger (2004), Remotely triggered seismicity on the United States West Coast following the Mw 7.9 Denali Fault earthquake, *Bull. Seismol. Soc. Am.*, *94*, S348–S359.

Purnell, P., N. Short, and C. Page (2001), A static fatigue model for the durability of glass reinforced cement, *J. Mater. Sci.*, *36*, 5385–5390.

Rathbun, A. P., and C. Marone (2010), Effect of strain localization on frictional behavior of sheared granular materials, *J. Geophys. Res.*, *115*, B01204, doi:10.1029/2009JB006466.

Reid, H. F. (1910), Mechanics of the earthquake, in *The California Earthquake of April 18, 1906: Report of the State Earthquake Investigation Commission*, vol. 2, pp. 16–28, Carnegie Inst. of Washington, Washington D. C.

Rice, J. R. (1983), Constitutive relations for fault slip and earthquake instabilities, *Pure Appl. Geophys.*, *121*(3), 443–475, doi:10.1007/BF02590151.

Richards, P. G. (1976), Dynamic motions near an earthquake fault: A three-dimensional solution, *Bull. Seismol. Soc. Am.*, *66*(1), 1–32.

Saito, M. (1969), Forecasting time of slope failure by tertiary creep, in *Proc. 7th Int. Conf. Soil Mech. and Found. Eng*, vol. 2, pp. 677–683, A.A. Balkema, Mexico City, Mexico.

Saito, M., and H. Uezawa (1961), Failure of soil due to creep, in *Proc. 5th Int. Conf. Soil Mech. and Found. Eng*, vol. 1, pp. 315–318, Dunod Press, Paris, France.
Salamon, M. D. G. (1970), Stability, instability and the design of pillar workings, *Int. J. Rock Mech. Min. Sci.*, *7*(6), 613–631.
Scholz, C. (1968), Mechanism of creep in brittle rock, *J. Geophys. Res.*, *73*, 3295–3302.
Scholz, C. (1972), Static fatigue of quartz, *J. Geophys. Res.*, *77*, 2104–2114.
Singh, D. P. (1975), A study of creep of rocks, *Int. J. Rock Mech. Min. Sci. Geomech. Abstr.*, *12*, 271–276.
Sinha, N. K., and S. Sinha (2005), Stress relaxation at high temperatures and the role of delayed elasticity, *Math. Sci. Eng. A*, *393*, 179–341.
Stein, S., and M. Liu (2009), Long aftershock sequences within continents and implications for earthquake hazard assessment, *Nature*, *462*, 87–89.
Turcotte, D. L., and R. Shcherbakov (2006), Can damage mechanics explain temporal scaling laws in brittle fracture and seismicity?, *Pure Appl. Geophys.*, *163*, 1031–1045.
Velasco, A. A., S. Hernandez, T. Parsons, and K. Pankow (2008), Global ubiquity of dynamic earthquake triggering, *Nat. Geosci.*, *1*, 375–379, doi:10.1038/ngeo204.
Voight, B. (1988a), A method for prediction of volcanic eruption, *Nature*, *332*, 125–130.
Voight, B. (1988b), Materials science laws applies to time forecast of slope failure, in *5th Int. Symp. Landslides Lausanne 1988*, vol. 3, edited by C. Bonnard, pp. 1471–1472, Balkema, Lausanne.
Voight, B. (1989), A relation to describe rate-dependent material failure, *Science*, *243*, 200–203.
Wiederhorn, S. M., and L. H. Bolz (1970), Stress corrosion and static fatigue of glass, *J. Am. Ceram. Soc.*, *50*, 543.